Materials Reports: Energy 3 (2023) 100180

Contents lists available at ScienceDirect

Materials Reports: Energy

journal homepage: www.keaipublishing.com/en/journals/materials-reports-energy

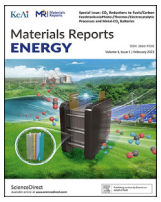

Original Research Report

Improving the activity of electrochemical reduction of CO_2 to C_1 products by oxidation derived copper catalyst

Lingxue Diao [a,1], Yingda Liu [a,1], Feifei Chen [a], Hong Pan [b], David Pérez de Lara [c], Hui Liu [a], Yahui Cheng [a,*], Feng Luo [d,**]

[a] Department of Electronic Science and Engineering and Tianjin Key Laboratory of Process Control and Green Technology for Pharmaceutical Industry, Nankai University, Tianjin, 300350, China
[b] Department of Basic Science, Tianjin Agricultural University, Tianjin, 300392, China
[c] IMDEA Nanosci, Faraday 9, Ciudad Univ Cantoblanco, Madrid, 28049, Spain
[d] Tianjin Key Lab for Rare Earth Materials and Applications, Center for Rare Earth and Inorganic Functional Materials, School of Materials Science and Engineering, Nankai University, Tianjin, 300350, China

ARTICLE INFO

Keywords:
Cu-based electrocatalyst
Electroreduction of CO_2
In-situ Raman spectra
C_1 product

ABSTRACT

Cu-based electrocatalysts have become the focus in the field of electrochemical CO_2 reduction reaction (ECO_2RR) due to their ability to produce multicarbon products. However, the research on generating single carbon products with higher economic feasibility via ECO_2RR based on Cu-based electrocatalysts is rather rare, and the roles of the surface architecture and oxides of the electrocatalysts have not been explained exactly. In this work, a two-step method including thermal oxidation and electroreduction is proposed to introduce Cu^+ into pure Cu foil to form Cu_2O/Cu electrocatalyst. By regulating the surface composition and morphology of the electrocatalyst in this way, the activity of ECO_2RR to C_1 products has been greatly improved. The Faradaic efficiency of carbon products of the Cu_2O/Cu electrode reaches 84% at −0.7 V vs. RHE with good selectivity for HCOOH and CO. The current density of Cu_2O/Cu electrode reaches −12.21 mA cm^{-2} at −0.8 V vs. RHE, which is much higher than that of the Cu foil electrode (−0.09 mA cm^{-2}). In-situ Raman characterization shows that Cu^+ in Cu_2O/Cu electrode could inhibit hydrogen generation and promote ECO_2RR by stabilizing the adsorption of CO_2.

1. Introduction

The continuous advance of industrialization and the accelerated consumption of fossil fuels have led to a sharp increase in atmospheric carbon dioxide (CO_2). At present, the concentration of CO_2 in the atmosphere reaches as high as 400 ppm, keeping an annual growth of 2.11%, which greatly influence the global carbon cycle.[1] Electrochemical CO_2 reduction reaction (ECO_2RR) is an effective way to mitigate CO_2 emission by converting CO_2 into value-added fuels to achieve carbon recycling.[2–8] While ECO_2RR is favorable, it comes at a significant large overpotential, poor selectivity and low energy efficiency.[5,8–12] Therefore, it is urgent to develop high-performance electrocatalysts and explore their catalytic mechanisms.

Cu-based electrocatalysts are the most widely studied due to their high catalytic activity, low cost, abundant reserves and easy modification.[6,8,9] Furthermore, they act as the key component to form C_{2+} products owing to their specific binding energy to *CO intermediates.[13] However, when used in ECO_2RR, Cu-based catalysts suffer from the problems of hydrogen side reaction, high overpotential and poor selectivity of carbon products.

Some studies have shown that the oxidation state on the surface of metal-based catalysts can reduce the activation barrier of CO_2, thereby

* Corresponding author.
** Corresponding author.
E-mail addresses: chengyahui@nankai.edu.cn (Y. Cheng), feng.luo@nankai.edu.cn (F. Luo).

Production and Hosting by Elsevier on behalf of KeAi

[1] Lingxue Diao and Yingda Liu contributed equally to this work.

https://doi.org/10.1016/j.matre.2023.100180
Received 10 November 2022; Received in revised form 18 January 2023; Accepted 25 January 2023
Available online 14 February 2023

improving the performance of ECO_2RR and solving the above-mentioned problems.[14] The Cu-based catalysts derived from Cu oxide or hydroxide, namely OD-Cu (oxidation derived Cu) catalysts, with Cu oxidation state retained on surface generally, exhibit excellent catalytic performance and attracted extensive attention.[14] Some findings have indicated that the presence of Cu^+ on the surface of OD-Cu would act as CO_2RR active site.[14] Moreover, OD-Cu catalysts hold more grain boundaries and the oxidation state of Cu, which are capable of stabilizing the activated CO_2 and the adsorbed intermediates on the surface of catalysts.[15–17] Cuenya and co-workers confirmed the survival of Cu^+ species on the surface of OD-Cu during ECO_2RR (−1.2 V vs. RHE) via operando X-ray absorption fine-structure spectroscopy (XAFS). They found that Cu^+ sites prevented the generation of CH_4, resulting in the selective generation of C_2H_4 with a Faradaic efficiency (FE) of up to 60% (−0.9 V vs. RHE).[18] In order to further understand the role of Cu^+, Goddard and co-workers studied the surface with adjacent Cu^+ and Cu^0 species through computational simulation, unveiling the capability of such surface in greatly reducing the energy barrier of CO_2 activation and promoting the *CO polymerization.[19] The above results demonstrated that the retention of a certain amount of Cu^+ on the surface of the Cu-based catalysts is an effective way to improve the reaction activity and product selectivity of the catalysts during ECO_2RR process.[20] However, most reported researches on OD-Cu were focused on improving its catalytic activity for generating C_{2+} products rather than C_1 products.

Compared with C_{2+} products, C_1 product has simple and small building-block molecules that can then be up-converted to a variety of products with lower energy consumption and higher economic feasibility.[21] In recent years, remarkable progress has been made in the ECO_2RR to C_1 products. In particular, the Faradaic efficiency of formic acid, formate, and carbon monoxide (CO) has exceeded 95% in many works.[22–28] It has been widely accepted that the catalysts based on Pd, Sn, Bi, In, Pb, etc. have high selectivity for formic acid and formate, while those based on Au, Ag, Pd, Zn, etc. have high selectivity for CO. In contrast, the performance of Cu-based catalysts, especially OD-Cu-based catalysts, in ECO_2RR to C_1 products is not prominent. Conflicts still exist,[29] and there is still a lack of in-situ tests to reveal the reaction process and mechanism. Therefore, the study on the performance and mechanism of OD-Cu in the ECO_2RR process is of great significance to developing Cu-based catalysts for C_1 production.

In this work, the OD-Cu catalysts were prepared by modifying the surface composition and structure of Cu foil electrode via a facile two-step method containing thermal oxidation and potentiostatic reduction. We found that some Cu^+ was introduced into the metal Cu, and a Cu_2O/Cu composite OD-Cu catalyst was formed after the sequential treatment of oxidation and reduction. The Cu_2O/Cu presents good selectivity for C_1 product, including gas product CO and liquid product HCOOH, and its activity for the ECO_2RR is greatly improved compared with that of the initial Cu foil. The FE of gas product CO reaches 39% at −0.4 V vs. RHE, and it still remains about 30% from −0.4 to −0.7 V vs. RHE during ECO_2RR. The FE of HCOOH reaches 52% at −0.7 V vs. RHE, and the total FE for CO_2RR reaches 84%. The mechanism of ECO_2RR was explored by in-situ Raman characterization. This simple method of modifying the surface morphology and structure of catalyst and in-situ characterization provide a new idea for the ECO_2RR research.

2. Experiment

2.1. Preparation of catalysts

The electrode was prepared by a two-step method, including thermal oxidation and electroreduction processes. First, Cu foil with the size of 0.8 × 2.0 cm^2 and thickness of 0.3 mm was ultrasonically cleaned in ethanol for 15 min to remove organic pollutants on the surface. Then, the Cu foil was heated in a quartz tube furnace under a mixed gas atmosphere of argon and oxygen with volume ratio of 200:3. The heating temperature of 950 °C is chosen to ensure good crystallinity, higher oxidation thickness, single film composition and stable surface of the obtained samples. When heating was conducted, the furnace temperature was first raised from room temperature to 950 °C within 20 min, and then maintained at 950 °C for 30 min. After natural cooling of the furnace to room temperature, the sample (marked as Cu_2O) could be obtained. Finally, the electroreduction treatment was carried out by processing the Cu_2O sample in 0.1 M CO_2-saturated $KHCO_3$ solution with potential of −0.3 V vs. RHE for 80 min, and the sample (marked as Cu_2O/Cu) was obtained.

2.2. Characterizations

The morphology and surface element distribution of Cu_2O, Cu_2O/Cu and Cu electrodes were characterized by field emission scanning electron microscopy (FE-SEM, JEOL JSM-6700F) equipped with an energy-dispersive spectroscopy (EDS). The phase was studied by X-ray diffractometer (XRD, Rigaku MiniFlexII), and Cu Kα was used as the radioactive source (λ = 0.15406 nm, 40 kV, 100 mA) with a scanning step of 0.02°. Transmission electron microscopic (TEM) images were recorded by transmission electron microscope (TEM, Tecnai G^2 F20). Before TEM measurements, the electroreduced Cu_2O/Cu sample was scraped off the electrode, dispersed into absolute ethanol and treated with ultrasound for 1.5 h. Drop the obtained suspension onto a nickel mesh, and place the nickel mesh on a filter paper and let it dry. Repeat this process 2 to 3 times, to obtain the sample used for TEM characterization. Chemical components and valence states were analyzed by X-ray photoelectron spectroscopy (XPS, PHI5000 Versa Probe, equipped with an Auger electron detector) with Al Kα X-ray source ($h\nu$ = 1486.8 eV). In-situ Raman spectroscopy was recorded on a micro-confocal Raman spectrometer (TEO SR-500I-A) with the 785 nm laser. The test wave number ranged from 180 to 2400 cm^{-1}. The Raman spectra of the corresponding samples were obtained under different potentials. During the in-situ Raman tests, ECO_2RR on Cu_2O/Cu electrode was performed in a home-made in-situ Raman cell with a quartz optical window. The reaction conditions in the in-situ Raman test process are the same as those in the electrochemical tests, and the CO_2 flow rate was maintained at 5 sccm. During the measurement, each potential lasted for 3 min and then each Raman spectrum was recorded with twenty accumulations over an acquisition time of 20 s.

2.3. Electrochemical tests

Electrochemical properties were characterized by a potentiostat/galfvanostat (CH Instruments, CHI660E and CHI760E) with a three-electrode configuration in an H-type electrolytic cell. The Cu_2O/Cu and Cu samples were used as working electrodes, Ag/AgCl in saturated KCl aqueous solution was used as reference electrode, platinum mesh was used as counter electrode, and the electrolyte environment was 0.1 M CO_2-saturated $KHCO_3$ solution (pH = 6.8). All the potentials in this work were converted into RHE scale using the Nernst equation $E_{RHE} = E_{Ag/AgCl} + 0.0591 \times pH + 0.197$. For chronoamperometry, a constant potential in the range of −0.3 ~ −0.8 V vs. RHE was applied. Electrochemical impedance measurements were carried out at 0 V vs. RHE with frequencies varying from 0.1 Hz to 1 MHz. Cyclic voltammograms were conducted from 0.40 to 0.5 V vs. RHE with a scan rate of 20, 40, 60, 80 and 100 mV s^{-1}, respectively. Electrochemical active surface area (ECSA) was estimated by the charge corresponding to Cu foil.

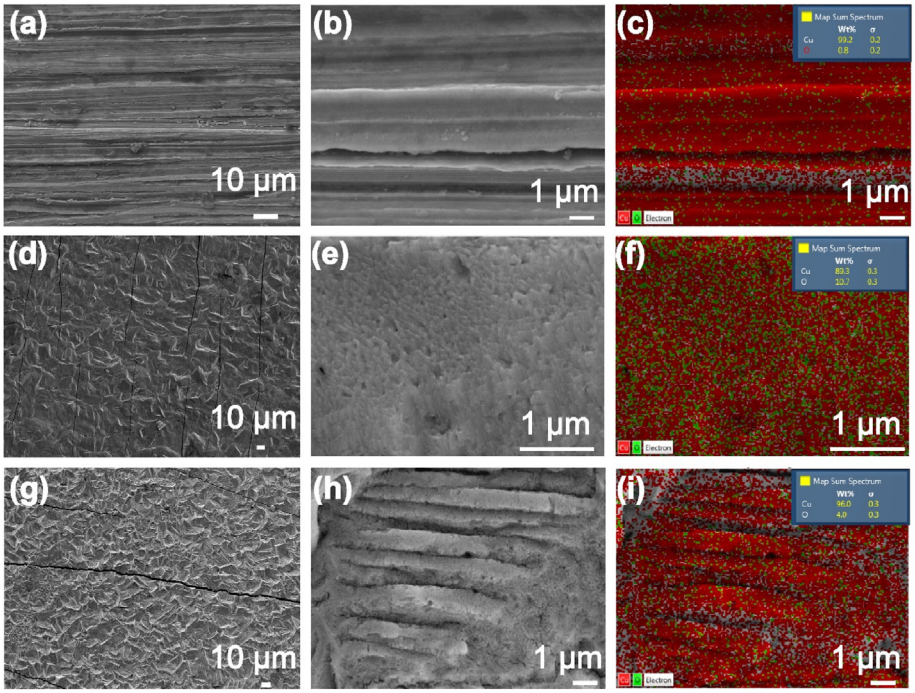

Fig. 1. (a) SEM image, (b) high-resolution SEM image and (c) element distribution (EDS) of Cu. (d) SEM image, (e) high-resolution SEM image and (f) EDS of Cu_2O. (g) SEM image, (h) high-resolution SEM image and (i) EDS of Cu_2O/Cu.

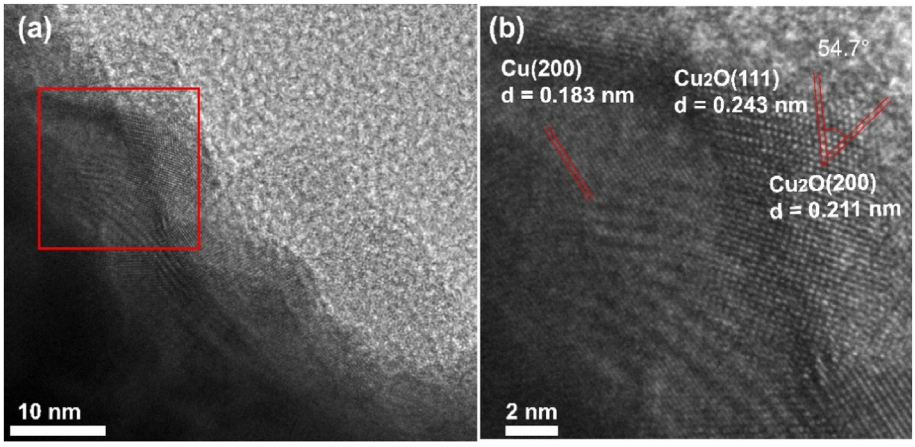

Fig. 2. (a) HRTEM image of Cu_2O/Cu sample. (b) Enlarged view of the area circled with red lines in (a).

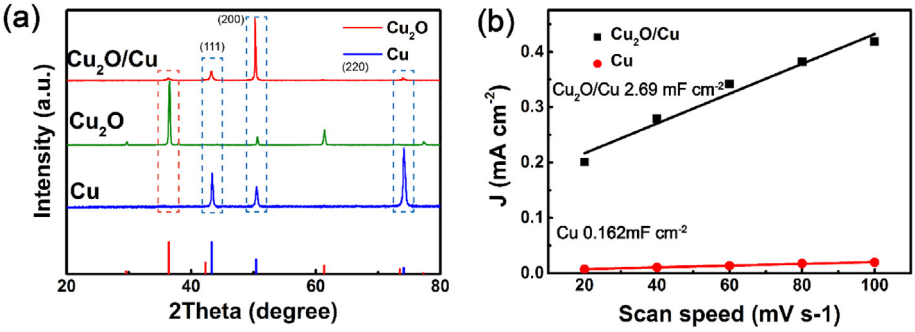

Fig. 3. (a) XRD patterns of Cu_2O/Cu, Cu_2O and Cu electrodes. (b) Charging current density differences plotted against the scan rates.

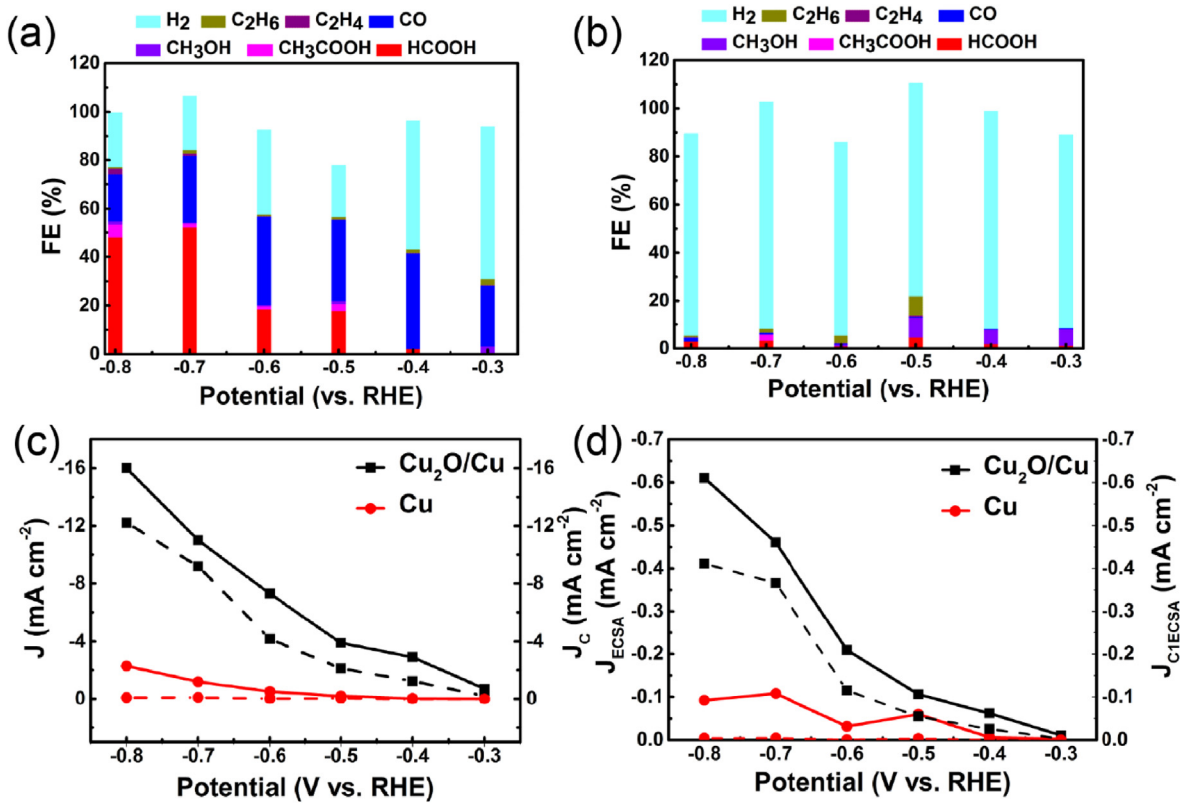

Fig. 4. Reduction products Faradaic efficiency (FE) of (a) Cu_2O/Cu electrode and (b) Cu electrode. (c) Reduction current density (*J*) curves and the current density for ECO_2RR (J_C, dotted line). (d) Active area normalized current density curves (J_{ECSA}) and the active area normalized current density curves of C_1 products (J_{C1ECSA}, dotted line).

2.4. ECO_2RR products analysis

The gas products were analyzed by gas chromatography (FULI, GC9790 Plus) in a gas-tight H-type electrolytic cell. The liquid products were collected and determined by proton nuclear magnetic resonance spectroscopy (^{1}H NMR, Bruker Avance AV III 400) by taking dimethylsulfoxide (DMSO) as a reference. 500 μL electrolyzed electrolyte, 10 μL DMSO (0.04 μL mL^{-1}) and 100 μL D_2O were thoroughly mixed and added into the nuclear magnetic tube to obtain ^{1}H spectrum.

3. Results and discussion

3.1. Structure, morphologies and composition

The morphologies and element distribution of Cu, Cu_2O and Cu_2O/Cu electrodes were characterized by scanning electron microscopy (SEM) and the results are shown in Fig. 1. It can be seen that the surface of Cu electrode is flat and smooth (Fig. 1a and b), and the surface of Cu_2O presents obvious pillar-shaped microcrystalline structure (Fig. 1d and e). The surface of Cu_2O/Cu electrode maintains the pillar-shaped microcrystalline structure after electroreduction process (Fig. 1g), and it presents a coarser surface with striped morphology compared with other two electrodes (Fig. 1h), which is conducive to increasing the active sites of the reaction.[20] In addition, according to the EDS results in Fig. 1c, f and i, Cu content in the samples follows the order of Cu_2O < Cu_2O/Cu < Cu, indicating that Cu_2O/Cu sample may consist of both Cu and Cu_2O phases after the process of thermal oxidation and electroreduction. The following XRD results can further confirm the existence of mixed phase of Cu.[11,12,30,31]

Fig. 2 shows the high-resolution transmission electron microscope (HRTEM) images of Cu_2O/Cu thin films, from which the lattice fringes of cubic Cu_2O and Cu can be clearly observed. The characteristic average lattice spacings of 0.243 nm and 0.211 nm given in Fig. 2b correspond to the cubic Cu_2O (111) and Cu_2O (200) crystal planes, respectively, and the included angle between the two crystal planes is 54.7°. In Fig. 2b, the crystal plane with the average lattice spacing of 0.183 nm corresponds to the cubic phase Cu (200) plane.

The as-prepared samples Cu_2O/Cu, Cu_2O and Cu were characterized by X-ray diffraction (XRD) and the results are shown in Fig. 3a. For Cu sample, the peaks at 43.32°, 50.45° and 74.12° are attributed to Cu (111), (200) and (220) crystal planes (PDF#85–1326), respectively. For Cu_2O sample, the characteristic peaks are assigned to the Cu_2O (PDF#05–0667) and the substrate Cu (PDF#05–0667). Among them, the peaks at 29.55°, 36.42°, 61.34° and 77.32° correspond to Cu_2O (110), (111), (220) and (222) crystal planes, respectively. The peak at 50.45° corresponds to Cu (200) crystal plane. The Cu_2O/Cu sample after electroreduction presents two phases, that is, Cu (PDF#05–0667) and Cu_2O (PDF#05–0667). The characteristic peak of Cu_2O is relatively weak, indicating that most of the electrode has been reduced to Cu.[6] Compared with the XRD standard pattern, the relative intensity of (200) crystal plane is significantly increased, indicating that Cu_2O/Cu sample has oriented growth.

X-ray photoelectron spectra (XPS) and Auger electron spectra (AES) were tested to further confirm the existence of Cu^+ at the surface of the Cu_2O/Cu sample. In the Cu LMM spectra in Fig. S1, it can be seen that the peak at 569.9 eV is attributed to Cu^+ of Cu_2O, and the peak at 568.1 eV is attributed to Cu^0 of metallic Cu. The results show that Cu^+ and Cu^0 coexist on the catalyst surface after electroreduction, which is consistent

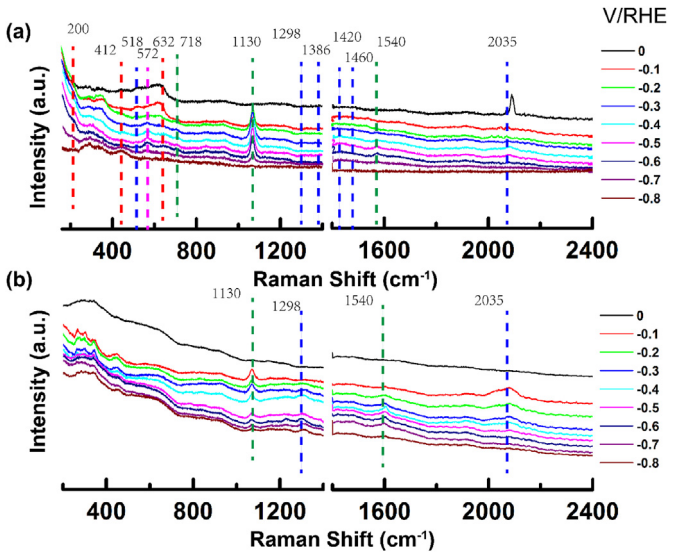

Fig. 5. Raman spectra of (a) Cu_2O/Cu electrode and (b) Cu electrode at different potentials.

with XRD results. The ratio of Cu^+:Cu^0 at the surface of Cu_2O/Cu is calculated to be 3.36:1 through fitting the Cu LMM spectra. The stable oxidation state of copper at negative potential may be attributed to the stable existence of oxygen within the amorphous subsurface of OD-Cu.[32]

The Cu_2O/Cu and Cu electrodes were tested by potential sweep cyclic voltammetry with different scanning speeds (from 20 to 100 mV s^{-1}) at the non-Faradaic potential region (Fig. S2). The double-layer capacitance of the electrodes can be estimated from the slope of the linear relationship in Fig. 3b. The capacitances of Cu_2O/Cu and Cu electrodes are 16.46 and 0.72 mF cm^{-2}, respectively. Obviously, the capacitance of Cu_2O/Cu electrode is approximately 17 times that of Cu electrode. Therefore, the active area of the electrode increases after the thermal oxidation and electroreduction processes, which is consistent with the result observed from SEM images.

3.2. ECO_2RR performance

ECO_2RR activities of Cu_2O/Cu and Cu electrodes were tested in a typical H-type electrolytic cell with 0.1 M CO_2-saturated $KHCO_3$ solution (pH = 6.8) as the electrolyte. In Fig. 4a and b, the Faradaic efficiency (FE) of carbon products for Cu_2O/Cu electrode is greatly improved compared with that of Cu electrode. Among the ECO_2RR products of Cu_2O/Cu electrode, the Faradaic efficiency of CO (FE_{CO}) reaches 39% at −0.4 V vs. RHE, realizing the high selection of CO products at low potential. The FE_{CO} is maintained at about 30% between −0.4 V and −0.7 V vs. RHE. In addition, the Faradaic efficiency of HCOOH (FE_{HCOOH}) is improved with the increasing bias potential, and it reaches 52% at −0.7 V vs. RHE, realizing the high selectivity of liquid products at low potential. The total FE of carbon products reaches 84% at −0.7 V vs. RHE. It should be noted that the Faradaic efficiency of CO and HCOOH tested repeatedly at different potentials has little fluctuation compared with the mean value under the continuous sampling test (Fig. S3), indirectly verifying the stability of the catalyst. In Fig. 4b, it can be seen that the main product of Cu electrode under negative bias is H_2. The highest FE of carbon product is only 22% at −0.5 V vs. RHE and it shows no selectivity for any carbon product. Fig. 4c and d summarize the current density for reaction (J), the current density for ECO_2RR (J_C), the active area normalized J_C (J_{ECSA}) and the active area normalized C_1 products current density (J_{C1ECSA}) with the application of bias voltage, respectively. It is obvious that J and J_C of Cu_2O/Cu electrode are much higher than that of Cu electrode. The J_C for

Table 1
Raman spectra peak positions and corresponding substances[16,29–31].

Raman shift (cm^{-1})	Assignment
200	Cu_2O[39]
412	Cu_2O[39]
518	*OCO[16]
572	Deformation (HO–H) of H_2O[16]
632	Cu_2O[38,39]
718	Deformation (O–C–O) of $*COO^{-3}$ [16]
1130	Symmetrical stretching (O–C–O) of $*COO^{-3}$ [16,40]
1298	Deformation (C–H) of *OCHO[16,40]
1386	Stretching (C–O) of *COOH[16]
1420 1460	Stretching (O–CH–O) of *OCHO[16,40]
1540	Antisymmetrical stretching (O–C–O) of $*COO^{-3}$ [16]
2035	Stretching of *C≡O, CO[16]

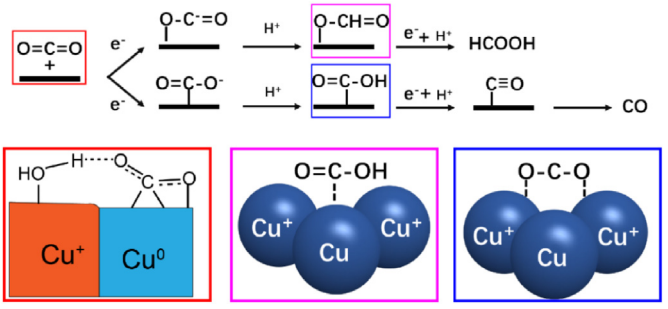

Fig. 6. Reaction paths of HCOOH and CO.

Cu_2O/Cu electrode reaches −12.21 mA cm^{-2} at −0.8 V vs. RHE, which is much higher than that of Cu electrode (−0.09 mA cm^{-2}). On one hand, the improvement of the ECO_2RR activity may be attributed to the increase of active area of Cu_2O/Cu electrode (Supplementary Material S2); on the other hand, it may be ascribed to the increase of intrinsic activity of Cu_2O/Cu electrode. As shown in Fig. 4d, after the normalization with active area, both the J_{ECSA} and J_{C1ECSA} of Cu_2O/Cu electrode are still much larger than that of Cu electrode within the potential range of −0.4 V to −0.7 V vs. RHE, proving the enhanced intrinsic activity of Cu_2O/Cu electrode. Here, the increase of intrinsic activity originates from the change of electrode surface structure and composition after treatment, such as the appearance of mixed valence state of Cu.[11,12,30–34] Through the above analysis, it can be concluded that the modified Cu_2O/Cu electrode performs higher activity and better selectivity for C_1 product compared with pure Cu electrode.

The stability of Cu_2O/Cu electrode was characterized by continuously testing current for 10 h at different potentials in the H-type electrolytic cell. The current was recorded and the gas products were extracted every hour. The gas composition was analyzed in the gas chromatograph, and the current density and Faradaic efficiency of carbon monoxide at each potential and each sampling moment were calculated. The stability test results are shown in Fig. S4. It can be seen that the current density stays stable during the 10-h continuous ECO_2RR test, and the absolute value of CO Faradaic efficiency fluctuated basically within 10% during the test.

3.3. Mechanism of ECO_2RR

In-situ characterization technologies are the common methods to characterize the changes of catalysts during the reaction process, so as to detect the active sites and the intermediate products to reveal the reaction path and the reaction mechanism.[35,36] In-situ Raman test was carried out in a customized electrolytic cell with 0.1 M CO_2-saturated $KHCO_3$ solution to understand the mechanism of ECO_2RR and the reason for improving the reduction activity and product selectivity of Cu_2O/Cu

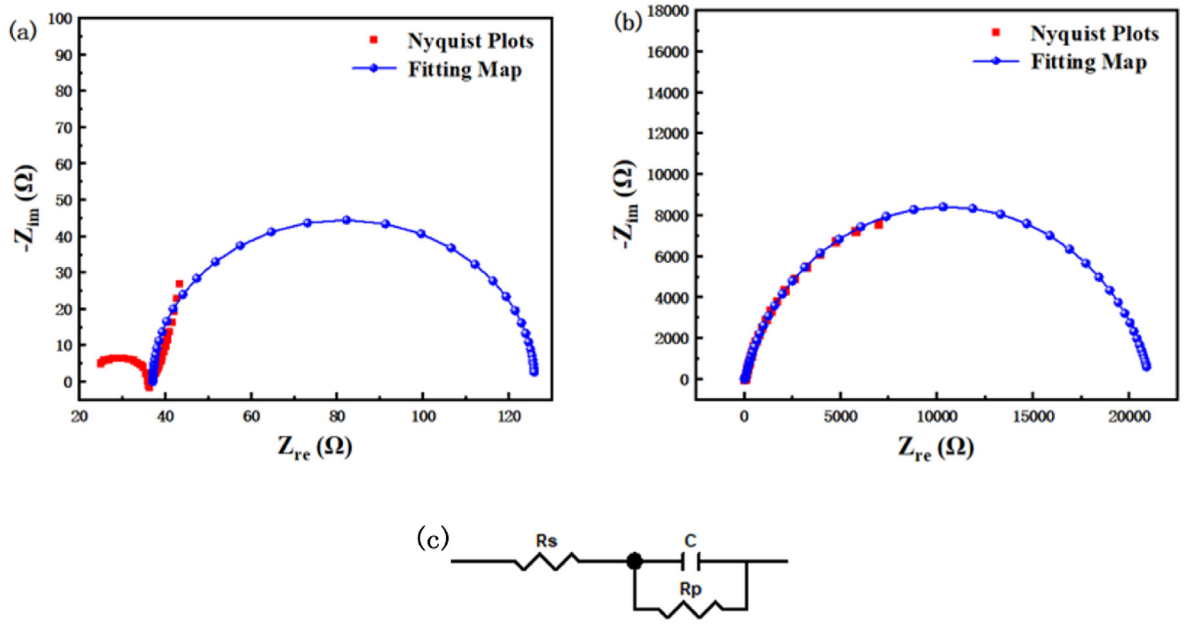

Fig. 7. Nyquist plots and the fitted spectra of (a) Cu_2O/Cu and (b) Cu. (c) Equivalent circuit model.

electrode. The Raman spectra are shown in Fig. 5, and the functional groups corresponding to the observed peaks are summarized in Table 1.[7,31,37,38] As can be seen in Fig. 5a and b, there are three sorts of Raman peaks, wherein the red peaks represent the characteristic peaks of Cu_2O electrode components, the green peaks represent the adsorption of CO_3^{2-}, and the blue peaks represent the adsorption of *OCHO, *COOH, *OCO and primary reduction intermediates. In Fig. 5a, some characteristic peaks of Cu^+ appear at 200, 412, 572 cm^{-1} on the surface of Cu_2O/Cu electrode, which is consistent with the previous SEM, XRD and TEM results. Besides, it shows that Cu^+ always exists in the range of −0.3 to −0.8 V vs. RHE during ECO_2RR, indicating the relative stability of Cu^+. Compared with Cu foil electrode, Cu_2O/Cu electrode shows a stronger peak at 1130 cm^{-1}, which corresponds to the adsorption of CO_3^{2-} on the electrode surface. This indicates that the OD-Cu electrode surface adsorbs more CO_3^{2-} and is more conducive to CO_2 activation. Cu_2O/Cu electrode exhibits more adsorption peaks of *OCHO, $*OCO^-$, *COOH and primary intermediates (Fig. 5a and b), further illustrating the superiority of Cu_2O/Cu electrode surface to the activation, adsorption and conversion of CO_2 compared with Cu foil electrode. From the above analysis, we can draw two conclusions: (i) Cu^+ still appears on the Cu_2O/Cu electrode surface during the process of ECO_2RR; (ii) Cu_2O/Cu electrode adsorbs and converts more CO_2, producing more intermediates than the original pure Cu electrode.

In Fig. 5a, *OCHO, $*OCO^-$, *COOH and the primary intermediates are probed on the surface of Cu_2O/Cu electrode. According to the above results, the reaction path of HCOOH and CO, as well as the main products of Cu_2O/Cu electrode are drawn and shown in Fig. 6. For HCOOH generation, CO_2 forms the $*OCO^-$ intermediate through the oxygen coordination on the Cu_2O/Cu electrode surface; after that, an H atom is added at the C-end to form the *OCHO intermediate; then, after coupling protons and transferring electrons, HCOOH is formed and desorbed. For CO generation, CO_2 is chemically adsorbed on the catalyst surface to form the $*COO^-$ intermediate through carbon coordination, and then H atom is added at the C-end to form *COOH; finally, CO is generated and desorbed from the catalyst surface.[40]

Compared with Cu electrode, Cu_2O/Cu electrode with mixed valence state of Cu is advantageous to adsorb more CO_2 for reaction.[19] Goddard et al. theoretically calculated the mixed interface of Cu^+/Cu^0 and found it conducive to activate CO_2. The calculation results show that the presence of Cu^+ sites at the mixed Cu^+/Cu^0 surface can bind H_2O molecules at the edge of Cu^0 region, and these H_2O molecules on the Cu^+ site form strong hydrogen bonds with CO_2 to stabilize the adsorbed CO_2 for further reaction (Fig. 6). In the Raman spectra in Fig. 5a, the peak at 572 cm^{-1} corresponds to the deformation vibration of HO–H, demonstrating the stronger H_2O adsorption and more CO_2 adsorption on mixed Cu^+/Cu^0 surface, which is consistent with the theoretical calculation results.[19] According to above analysis, we come to a conclusion that the mixed Cu^+/Cu^0 surface on the Cu_2O/Cu electrode can promote ECO_2RR and inhabit hydrogen evolution by stabilizing the adsorbed CO_2.[40]

In order to further understand the mechanism of Cu_2O/Cu electrode accelerating the reaction process, electrochemical impedance spectroscopy (EIS) was also conducted, and the Nyquist plots were obtained by running at 0 V vs. RHE. Fig. 7a and b shows the EIS impedance spectra and their fitted spectra of Cu_2O/Cu and Cu, respectively. The equivalent circuit fitting is carried out according to the model shown in Fig. 7c. Based on the fitting parameters, it can be calculated that the charge transfer resistance of Cu_2O/Cu is about 88.82 Ω, while that of pure Cu is about 21016 Ω. The charge transfer resistance of Cu_2O/Cu is greatly reduced, and electron transfer on Cu_2O/Cu electrode is easier than that on Cu electrode, which is related to the existence of Cu_2O/Cu interface in the electrode.[19]

The above results show that the Cu^+/Cu^0 hybrid interface is conducive to CO_2 activation to produce primary products, which provides ideas for subsequent catalysts design. It is worth mentioning that the synthesis of C_{2+} products is still the future goal. Some additional efforts are required to promote the formation of C_{2+} products, such as providing higher reduction potential, improving the diffusion and mass transfer of CO, constructing three-dimensional microstructure to improve the confinement of intermediates, etc., which should be considered and improved in the future.

4. Conclusion

In this work, Cu_2O/Cu electrode was prepared by a facile thermal oxidation-electroreduction method, which improved the activity of ECO_2RR and realized the high selectivity of C_1 product. This simple method changes both surface morphology and components of Cu-based electrode to form an OD-Cu film with mixed Cu^+/Cu^0, which increases the active area, improves intrinsic activity of ECO_2RR and inhabits hydrogen evolution. In-situ Raman spectra results show that the OD-Cu

electrode can adsorb more CO_2 and generate more primary intermediates. In addition, the Cu^+ existing on the surface of Cu_2O/Cu electrode is conductive to CO_2 activation, which further proves the great effect of electrode composition on products selectivity. This simple method provides a new idea to improve the performance of Cu-based ECO_2RR catalyst.

Declaration of competing interest

The authors declare that they have no known competing financial interests or personal relationships that could have appeared to influence the work reported in this paper.

Acknowledgments

This work was supported by National Natural Science Foundation of China (No. 52071183).

Appendix A. Supplementary data

Supplementary data to this article can be found online at https://doi.org/10.1016/j.matre.2023.100180.

References

1. Raciti D, Wang Y, Park JH, et al. Three-dimensional hierarchical copper-based nanostructures as advanced electrocatalysts for CO_2 reduction. *ACS Appl Energy Mater*. 2020;1:2392–2398.
2. Albo J, Sáez A, Solla-Gullón J, et al. Production of methanol from CO_2 electroreduction at Cu_2O and Cu_2O/ZnO-based electrodes in aqueous solution. *Appl Catal, B*. 2015;176:709–717.
3. Zhu Q, Sun X, Yang D, et al. Carbon dioxide electroreduction to C_2 products over copper-cuprous oxide derived from electro-synthesized copper complex. *Nat Commun*. 2019;10:1–11.
4. Bagger A, Ju W, Varela AS, et al. Electrochemical CO_2 reduction: a classification problem. *ChemPhysChem*. 2017;18:3266–3273.
5. Raciti D, Livi KJ, Wang C. Highly dense Cu nanowires for low-overpotential CO_2 reduction. *Nano Lett*. 2015;15:6829–6835.
6. Ji S, Qu Y, Wang T, et al. Rare-earth single erbium atoms for enhanced photocatalytic CO_2 reduction. *Angew Chem*. 2020;132:10738–10744.
7. Wang Z, Akter Monny S, Wang L. Hollow structure for photocatalytic CO_2 reduction. *ChemNanoMat*. 2020;6:881–888.
8. Wang H, Wang Y, Guo L, et al. Solar-heating boosted catalytic reduction of CO_2 under full-solar spectrum. *Chin J Catal*. 2020;41:131–139.
9. Lin R, Guo J, Li X, et al. Electrochemical reactors for CO_2 conversion. *Catalysts*. 2020;10:473.
10. Li XQ, Duan GY, Chen JW, et al. Regulating electrochemical CO_2RR selectivity at industrial current densities by structuring copper@poly (ionic liquid) interface. *Appl Catal B Environ*. 2021;297, 120471.
11. Xie H, Wang T, Liang J, et al. Cu-based nanocatalysts for electrochemical reduction of CO_2. *Nano Today*. 2018;21:41–54.
12. Li XQ, Duan GY, Chen JW, et al. Regulating electrochemical CO_2RR selectivity at industrial current densities by structuring copper@poly (ionic liquid) interface. *Appl Catal B Environ*. 2021;297, 120471.
13. Nitopi S, Bertheussen E, Scott SB, et al. Progress and perspectives of electrochemical CO_2 reduction on copper in aqueous electrolyte. *Chem Rev (Washington, DC, U S)*. 2019;119:7610–7672.
14. Wu ZZ, Gao FY, Gao MR. Regulating the oxidation state of nanomaterials for electrocatalytic CO_2 reduction. *Energy Environ Sci*. 2021;14:1121–1139.
15. Jeon HS, Sinev I, Scholten F, et al. Operando evolution of the structure and oxidation state of size-controlled Zn nanoparticles during CO_2 electroreduction. *J Am Chem Soc*. 2018;140:9383–9386.
16. Shan W, Liu R, Zhao H, et al. In situ surface-enhanced Raman spectroscopic evidence on the origin of selectivity in CO_2 electrocatalytic reduction. *ACS Nano*. 2020;14:11363–11372.
17. Gao S, Lin Y, Jiao X, et al. Partially oxidized atomic cobalt layers for carbon dioxide electroreduction to liquid fuel. *Nature*. 2016;529:68–71.
18. Mistry H, Varela AS, Bonifacio CS, et al. Highly selective plasma-activated copper catalysts for carbon dioxide reduction to ethylene. *Nat Commun*. 2016;7:1–9.
19. Xiao H, Goddard WA, Cheng T, et al. Cu metal embedded in oxidized matrix catalyst to promote CO_2 activation and CO dimerization for electrochemical reduction of CO_2. *Proc Natl Acad Sci USA*. 2017;114:6685–6688.
20. Kong T, Jiang Y, Xiong Y. Photocatalytic CO_2 conversion: what can we learn from conventional CO_x hydrogenation? *Chem Soc Rev*. 2020;49:6579–6591.
21. Bushuyev OS, de Luna P, Dinh CT, et al. What should we make with CO_2 and how can we make it? *Joule*. 2018;2:825–832, 27.
22. Lei Y, Wang Z, Bao A, et al. Recent advances on electrocatalytic CO_2 reduction to resources: target products, reaction pathways and typical catalysts. *Chem Eng J*. 2023;453, 139663.
23. Li J, Zhang Z, Hu W. Exclusive CO_2-to-formate conversion over single-atom alloyed Cu-based catalysts. *Green Energy & Environment*. 2022;7:855–857.
24. Wang X, Liu S, Zhang H, et al. Polycrystalline SnS_x nanofilm enables CO_2 electroreduction to formate with high current density. *Chem Commun*. 2022;58:7654–7657.
25. Wen G, Lee DU, Ren B, et al. Orbital interactions in Bi-Sn bimetallic electrocatalysts for highly selective electrochemical CO_2 reduction toward formate production. *Adv Energy Mater*. 2018;8, 1802427.
26. Guo J-H, Zhang X-Y, Dao X-Y, et al. Nanoporous metal-organic framework-based ellipsoidal nanoparticles for the catalytic electroreduction of CO_2. *ACS Appl Nano Mater*. 2020;3:2625–2635.
27. Ren W, Tan X, Yang W, et al. Isolated diatomic Ni-Fe metal-nitrogen sites for synergistic electroreduction of CO_2. *Angew Chem Int Ed*. 2019;58:6972–6976.
28. Feng J, Gao H, Zheng L, et al. A Mn-N_3 single-atom catalyst embedded in graphitic carbon nitride for efficient CO_2 electroreduction. *Nat Commun*. 2020;11:4341.
29. Chen H, Wang Z, Cao S, et al. Facile synthesis of an antimony-doped Cu/Cu_2O catalyst with robust CO production in a broad range of potentials for CO_2 electrochemical reduction. *J Mater Chem A*. 2021;9, 23234.
30. Todorova TK, Schreiber MW, Fontecave M. Mechanistic understanding of CO_2 reduction reaction (CO_2RR) toward multicarbon products by heterogeneous copper-based catalysts. *ACS Catal*. 2019;10:1754–1768.
31. Luo W, Xie W, Mutschler R, et al. Selective and stable electroreduction of CO_2 to CO at the copper/indium interface. *ACS Catal*. 2018;8:6571–6581.
32. Cavalca F, Ferrgut R, Aghion S, et al. Nature and distribution of stable subsurface oxygen in copper electrodes during electrochemical CO_2 reduction. *J Phys Chem C*. 2017;121:25003–25009.
33. Wan L, Zhou Q, Wang X, et al. Cu_2O nanocubes with mixed oxidation-state facets for (photo) catalytic hydrogenation of carbon dioxide. *Nature Catalysis*. 2019;2:889–898.
34. Kim D, Lee S, Ocon JD, et al. Insights into an autonomously formed oxygen-evacuated Cu_2O electrode for the selective production of C_2H_4 from CO_2. *Phys Chem Chem Phys*. 2015;17:824–830.
35. Dutta A, Kuzume A, Rahaman M, et al. Monitoring the chemical state of catalysts for CO_2 electroreduction: an in operando study. *ACS Catal*. 2015;5:7498–7502.
36. Luo W, Zhang Q, Zhang J, et al. Electrochemical reconstruction of ZnO for selective reduction of CO_2 to CO. *Appl Catal B Environ*. 2020;273, 119060.
37. Lee SY, Jung H, Kim NK, et al. Mixed copper states in anodized Cu electrocatalyst for stable and selective ethylene production from CO_2 reduction. *J Am Chem Soc*. 2018;140:8681–8689.
38. Yang H, Hu Y, Chen J, et al. Intermediates adsorption engineering of CO_2 electroreduction reaction in highly selective heterostructure Cu-based electrocatalysts for CO production. *Adv Energy Mater*. 2019;9, 1901396.
39. Yu L, Li G, Zhang X, et al. Enhanced activity and stability of carbon-decorated cuprous oxide mesoporous nanorods for CO_2 reduction in artificial photosynthesis. *ACS Catal*. 2016;6:6444–6454.
40. Wang X, Gao C, Low J, et al. Efficient photoelectrochemical CO_2 conversion for selective acetic acid production. *Sci Bull*. 2021;66:1296–1304.

Lingxue Diao received her BS degree in Shandong Jianzhu University in 2019. Currently, she is a postgraduate student at Nankai University supervised by Prof. Yahui Cheng and Prof. Hui Liu. Her research direction is focused on the Cu-based photocatalysts/elecrocatalysts for CO_2 reduction and water splitting.

Yingda Liu received his BS degree from Northeastern University in 2020. Currently, he is a postgraduate student at Nankai University supervised by Prof. Yahui Cheng. His research direction is focused on the copper single crystal electrocatalyst for CO_2 reduction.

Yahui Cheng is a Professor at Nankai University, China. She received her BS and MS degrees from Tianjin University, her PhD in Physical Electronics from Nankai University, and her post-doctoral training from the University of Sydney. Her current research interests are on advanced energy/environmental electrochemistry and photoelectrochemistry, including CO_2 reduction, water splitting and pollutant degradation.

Feng Luo is a professor at Nankai University, China. He received the BS and PhD degree from College of Chemistry and Molecular Engineering, Peking University (supervisor: Prof. Chunhua Yan). He is the member of Institute of Science and Innovation Commission, Advanced Science Facilities, Shenzhen, and Shanghai Synchrotron Radiation Facility User Commission. He is also the second prize winner of the 9th Overseas Chinese Contribution Award. He has long been engaged in the synthesis, characterization and performance analysis of rare earth oxide functional thin films, rare earth two-dimensional layered materials, and rare earth-precious metal-transition metal multi-component high entropy alloy nanomaterials. He is good at analyzing the microstructure and the structure–activity relationship of spin–induced catalysis using synchrotron radiation source in situ characterization technology and 4D in situ electron microscopy technology. He has presided over the Spanish Outstanding Youth Fund, the Spanish General Fund and presided/participated in a number of Major Program of the National Natural Science Foundation of China, Major Nanomanufacturing Plan of the National Natural Science Foundation of China, and Key Research and Development Program of the Ministry of Science and Technology, and Key Research and Development Program of Ministry of Science and Technology.